Antibacterial marinopyrroles and pseudilins act as protonophores

Gabriel Castro-Falcón[1], Jan Straetener[2], Jan Bornikoel[2], Daniela Reimer[1], Trevor N. Purdy[1], Florence M. Schempp[1], Dennis Y. Liu[3], Roger G. Linington[3], Heike Brötz-Oesterhelt[2,4,5,*], Chambers C. Hughes[1,2,4,5,*]

[1]Center for Marine Biotechnology and Biomedicine, Scripps Institution of Oceanography, University of California, San Diego, California 92093, USA

[2]Department of Microbial Bioactive Compounds, Interfaculty Institute of Microbiology and Infection Medicine, University of Tübingen, 72076 Tübingen, Germany

[3]Department of Chemistry, Simon Fraser University, Burnaby, British Columbia V5A 1S6, Canada

[4]Cluster of Excellence EXC 2124: Controlling Microbes to Fight Infection, University of Tübingen, 72076 Tübingen, Germany

[5]German Center for Infection Research, Partner Site Tübingen, 72076 Tübingen, Germany

heike.broetz-oesterhelt@uni-tuebingen.de

chambers.hughes@uni-tuebingen.de

1

Abstract

Elucidating the mechanism of action (MoA) of antibacterial natural products is crucial to evaluating their potential as novel antibiotics. The marinopyrroles, pentachloropseudilin, and pentabromopseudilin are densely halogenated, hybrid pyrrole-phenol natural products with potent activity against Gram-positive bacterial pathogens like *Staphylococcus aureus*. However, the exact way in which they exert this antibacterial activity has not been established. In this study, we explore their structure-activity relationship, determine their spatial location in bacterial cells, and investigate their MoA. We show that the natural products share a common MoA based on membrane depolarization and dissipation of the proton motive force (PMF) that is essential for cell viability. The compounds show potent protonophore activity, but do not appear to destroy the integrity of the cytoplasmic membrane via the formation of larger pores or interfere with the stability of the peptidoglycan sacculus. Thus, our current model for the antibacterial MoA of marinopyrrole, pentachloropseudilin, and pentabromopseudilin stipulates that the acidic compounds insert into the membrane and transport protons inside the cell. This MoA may explain many of the deleterious biological effects in mammalian cells, plants, phytoplankton, viruses, and protozoans that have been reported for these compounds.

2

TOC GRAPHIC:
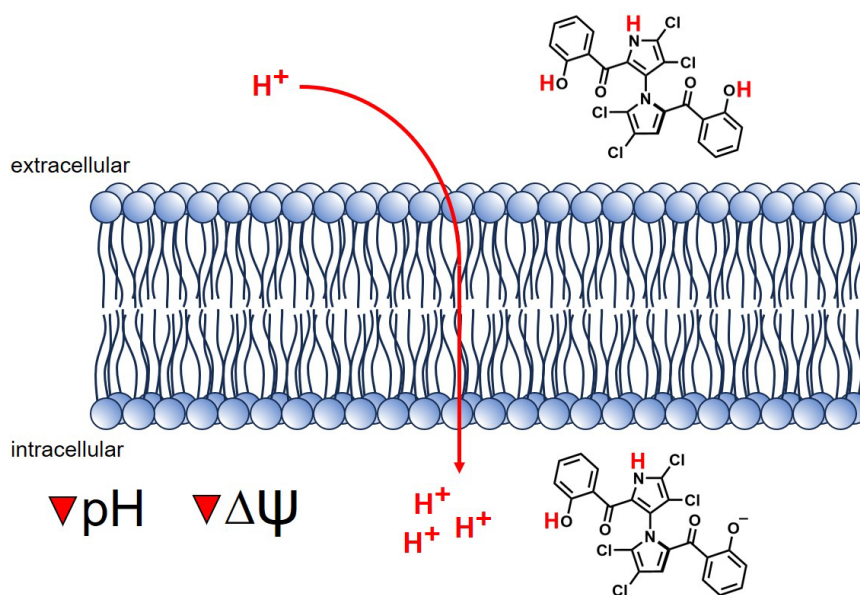
Marinopyrrole A (MarA, **1**),[1] pentabromopseudilin (PBP, **2**),[2,3] and pentachloropseudilin (PCP, **3**)[4,5] are densely halogenated hybrid pyrrole-phenol natural products isolated from various bacteria (Figure 1). Since the compounds have pronounced cytotoxicity against cancer cell lines, various studies have focused on the anti-eukaryotic properties of **1-3**, wherein actin,[6] Mcl-1,[7] and others[8] have been identified as eukaryotic targets for MarA (**1**), myosin for PBP (**2**) and PCP (**3**),[9–11] and human lipoxygenases 15-hLO and 12-hLO for **2**.[12] However, the conclusion that **1** is a selective Mcl-1 inhibitor has been called into question.[13,14] Various reports detailing the deleterious biological effects of **1-3** in mammalian cells,[15] plants,[16] phytoplankton,[17] viruses,[18] and parasitic protozoans[19–21] continue to be disclosed. Although the original reports of these unusual compounds were tied to their antibacterial activity, where they uniformly showed potent activity against Gram-positive pathogens and little or no activity against Gram-negative pathogens,[22,23] little work regarding their antibacterial mode of action has been reported.

We therefore initiated a project with the aim of uncovering the antibacterial mode of action of **1**-**3**. Notably, in 2013, we proposed that PCP's mode of action involved protein synthesis inhibition, perhaps via inhibition of a bacterial ATPase, using high-content bacterial imaging.[24] Since then, several reports with structurally-similar, densely halogenated pyrrole- and phenol-containing compounds, such as the pyrrolomycins,[25] mindapyrroles,[26] and armeniaspirol,[27] have strongly indicated that **1-3** may act as protonophores. Nonetheless, a study that specifically addresses this question in live bacterial cells, one that is ideally in agreement with several papers examining the structure-activity relationships of the compounds,[16,28–30] is lacking.
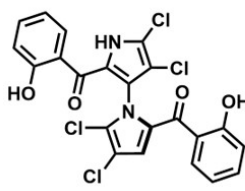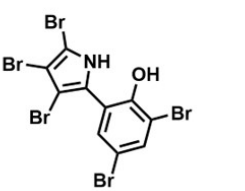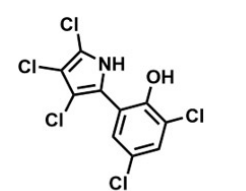
4

Figure 1. Structures of marinopyrrole A (**1**), pentabromopseudilin (**2**), and pentachloropseudilin (**3**), including the original bacterial producer strain, reported biological activities, and reported cellular targets. Mcl-1 = myeloid cell leukemia 1; IspD = 2-C-methyl-D-erythritol 4-phosphate cytidylyltransferase.

Results and Discussion

Antibacterial Activity

First, we assessed the antibacterial activity of (±)-**1**–**3** against an extensive panel of bacterial species including both Gram-positive and Gram-negative pathogens at the Centre for High-Throughput Chemical Biology at Simon Fraser University (Supplementary Tables S1 and S2). In general, the compounds showed broad but weak activity against Gram-negative pathogens (e.g., *Escherichia coli*, *Klebiella aerogenes*, *Klebsiella pneumoniae*, *Acinetobacter baumannii*, *Pseudomonas aeruginosa*, *Vibrio cholerae*). However, against Gram-positive pathogens (e.g., *Bacillus subtilis*, *Staphylococcus epidermidis*, *Staphylococcus aureus*, *Streptococcus pneumoniae*) the natural products showed mostly sub-μM minimum inhibitory concentrations (MICs) (Supplementary Table S1), which is consistent with previous studies

5

assessing the antibacterial activities of these compounds.[1,22,23] We followed up on these results by determining MICs against two model strains, *S. aureus* NCTC8325 and *B. subtilis* 168, to be used in our mode of action studies (Figure 2). Here, MarA (**1**) showed an MIC of 0.25 and 0.125 µg mL^{-1} against the respective bacterial strains and pentabromopseudilin (**2**) and pentachloropseudilin (**3**) were particularly potent; the former gave MICs of 0.016 µg mL^{-1} against both strains and the latter MICs of 0.004 µg mL^{-1}. The activity was not specific to prokaryotes, as **1**–**3** also showed significant cytotoxicity (Figure 2) against the cancer cell lines HeLa (human cervix epithelial carcinoma, IC$_{50}$ 0.63–4.20 µg mL^{-1}) and A549 (human lung epithelial carcinoma, IC$_{50}$ 4.17–13.63 µg mL^{-1}) as well as the non-cancerous MRC5 (human fetal lung fibroblast, IC$_{50}$ 0.15–1.69 µg mL^{-1}) cell line. The overall trend in cytotoxicity (PCP > PCB > MarA) mirrored the observed trend in antibacterial activity, which might suggest a common mode of action for both cell types.

We explored the structure-activity relationship using several synthetic compounds focusing on the presence and absence of the halogen atoms and the polar N-H and O-H functional groups. Although monodeoxypyoluteorin (**4**), which corresponds to the monomer of MarA, showed some residual antibacterial activity against *S. aureus* NCTC8325 and *B. subtilis* 168 (MIC 2 µg mL^{-1} and 16 µg mL^{-1}), the nonhalogenated synthetic compounds **5**, **6**, and **7** were devoid of activity. Considering a specific interaction with a protein target, this result could point toward a key role for the halogen atoms with regards to target affinity and antibacterial activity, such as electrostatic halogen bonding interactions. Partial methylation of MarA (**1**) gave O,O'-dimethyl MarA (**8**), which displayed greatly diminished antibacterial activity compared to the natural product. Full methylation gave O,O',N-trimethyl MarA (**9**), which showed no measurable antibacterial activity. Along the same lines, this result could indicate key hydrogen-bonding interactions between MarA and its bacterial target(s).

6

A

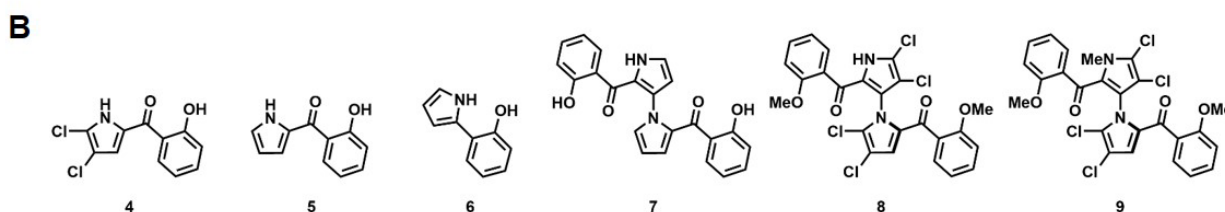|	MIC (µg mL^{-1})		IC$_{50}$ (µg mL^{-1})		
	S. aureus NCTC8325	*B. subtilis* 168	HeLa	A549	MRC5
MarA (**1**)	**0.25**	**0.125**	4.2	14	1.7
PBP (**2**)	**0.016**	**0.016**	1.1	6.4	0.28
PCP (**3**)	**0.004**	**0.004**	0.63	4.2	0.15
monodeoxypyoluteorin (**4**)	2	16	13	54	6.7
pyrrole **5**	>64	>64	>64	>64	>64
pyrrole **6**	32	>64	>64	>64	>64
dipyrrole **7**	32	>64	7.1	27	15
dimethyl MarA (**8**)	8	32	22	37	44
trimethyl MarA (**9**)	>64	>64	>64	>64	>64
control	1	0.25	0.11	1.2	0.92

B

Figure 2. Antibacterial and cytotoxic activities of compounds **1**–**9**. A) MICs of **1**–**9** against *S. aureus* NCTC8325 and *B. subtilis* 168 and half maximal inhibitory concentrations (IC$_{50}$s) against HeLa, A549, and MRC5 eukaryotic cells. Control = vancomycin (MIC) for the antibacterial assay and mitoxanthrone (IC$_{50}$) for the cytotoxicy assay. The section in grey highlights the potent antibacterial activity of the natural products (**1**–**3**). B) Structures of **4**–**9**. MarA = marinopyrrole A; PBP = pentabromopseudilin; PCP = pentachloropseudilin.

Cellular Localization of Coumarin Probes and Membrane Dyes

In order to elucidate the cellular mechanism of natural products **1-3**, we first explored their localization in bacterial cells. HATU-mediated ester coupling of **1-7** with 6-heptynoic acid produced alkynes that were subsequently appended to a fluorescent coumarin azide via copper-catalyzed click reaction. The coumarin itself was prepared via amide coupling of 3-azido-1-propanamine and 2-(7-(dimethylamino)-2-oxo-2H-chromen-4-yl)acetic acid. The corresponding

7

coumarins **1C**-**7C** were strictly characterized by ^{1}H and ^{13}C NMR spectroscopy, including HSQC and HMBC experiments to determine the exact position of the fluorescent tag (Figure 3A) (Supplementary Tables S3-S5, Supplementary Figures S1-33). In terms of their activity against *B. subtilis* 168, the coumarin derivatives were 6-60 times less active than the unmodified natural products and some maintained considerable antibacterial activity (**1C**: 0.83 µg mL^{-1}; **2C**: 0.25 µg mL^{-1}; **3C**: 0.25 µg mL^{-1}). As expected, coumarin **10** and **11** displayed no significant antibacterial activity against *B. subtilis* 168 (MIC >64 µg mL^{-1}).

Fluorescence images of *B. subtilis* 168 cells treated with **1C**-**3C** showed different fluorescence intensities but a similar nonuniform localization with bright, irregular signals in the cell periphery and in the septal cell area (Figure 3B). This phenotype, shared by all three natural products, was reminiscent of the distribution of widely-used membrane dyes in cells exposed to membrane-active agents.[31,32] Indeed, when *B. subtilis* 168 cells were treated with the (unlabeled) natural products **1**–**3** followed by staining with the membrane dye FM 5-95, the images showed the same phenotype as the ones generated with **1C**-**3C** (Figure 3C). The aggregated, inhomogenous, "spotty" localization of the membrane dye FM 5-95 can also be generated by exposure of *B. subtilis* to the protonophore m-chlorophenyl hydrazone (CCCP), which we selected for comparison (Figure 3C). This phenotype provided the first hint that the bacterial membrane is the target of **1**-**3**.
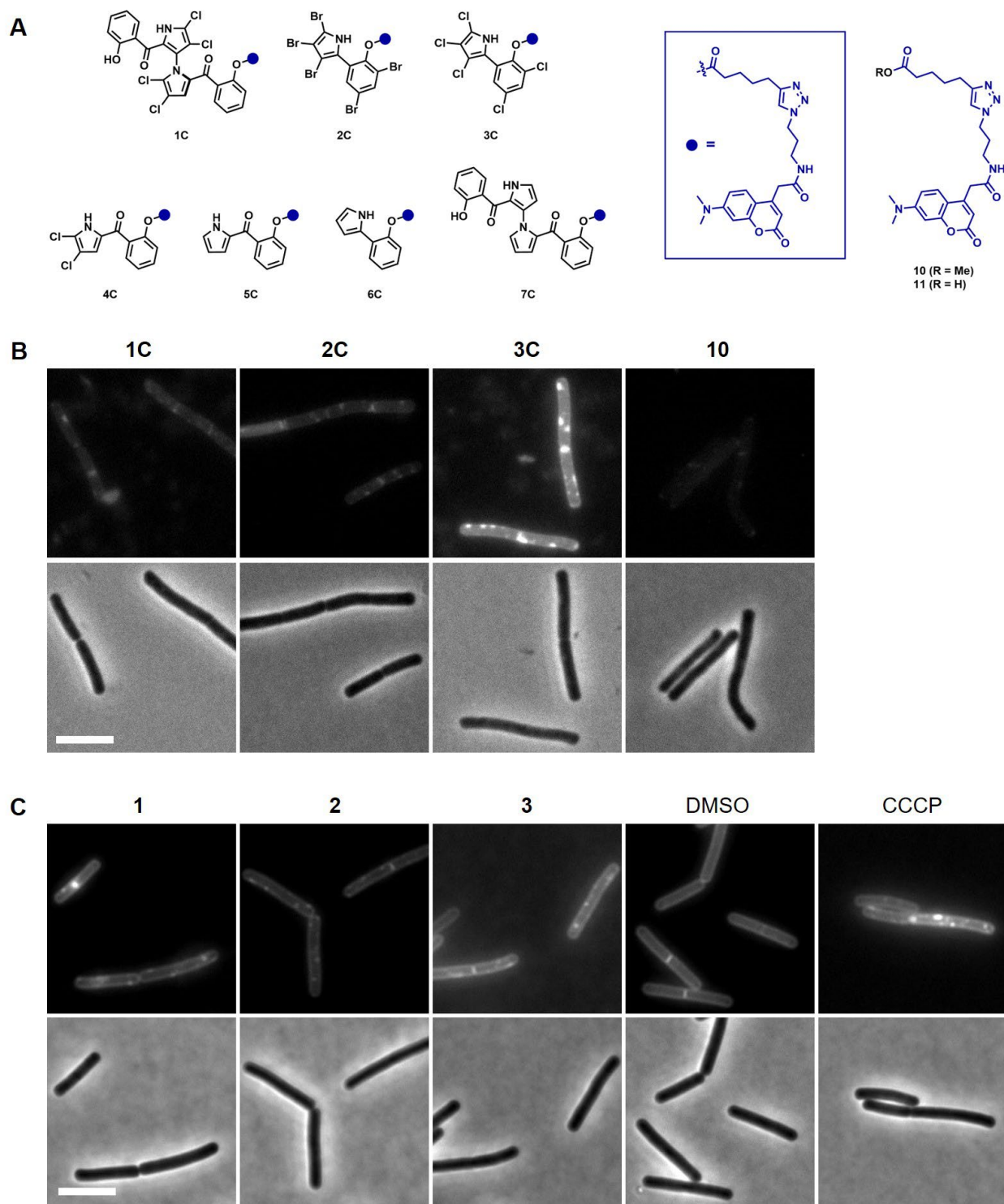
Figure 3. Cellular localization of coumarin probes and membrane dye FM 5-95. A) Structures of **1C-7C**, **10**, and **11**. B) *B. subtilis* 168 cells incubated with **1C** (1 µg mL^{-1}, 1x MIC), **2C** (0.25 µg mL^{-1}, 1x MIC) or **3C** (0.25 µg mL^{-1}, 1x MIC) for 10 minutes. Coumarin **10** (8 µg mL^{-1}) was used

as a negative control. The top row shows the fluorescence channel and the bottom row shows the phase-contrast images. The micrographs display representative images of three biological replicates. All images in 3B were adjusted to the same microscopy settings for direct qualitative comparison. Scale bar, 5 µm. C) *B. subtilis* 168 cells incubated with **1** (0.125 µg mL^{-1}, 1x MIC), **2** (0.016 µg mL^{-1}, 1x MIC) and **3** (0.004 µg mL^{-1}, 1x MIC) for 15 minutes and then stained with the membrane dye FM5-95 (20 µg mL^{-1}). DMSO (1%) was used as a negative control, and CCCP (100 µM) as a positive control. The top row shows the fluorescence channel, and the bottom row shows the phase-contrast images. The images displayed are representative of two biological replicates and are all adjusted to the same setting for qualitative comparison. Scale bar, 5 µm. CCCP = carbonyl cyanide m-chlorophenyl hydrazone.

Protonophore Activity

In addition to their possible role in target affinity, the removal of halogen atoms and the derivatization of N-H and O-H groups, which had a significant effect on antibacterial activity, both serve to decrease the overall acidity of the phenolic compounds (see Figure 2). Hydrophobic compounds bearing acidic functionality can act simply as protonophores and disrupt the proton gradient across cell membranes by active, protein-decoupled transport of protons across the membrane.[31,33] The lower pH directly outside the cell membrane is essential for cell viability as the passage of protons into the cell is coupled to important cellular processes like ATP synthesis and active transport of certain molecules across the membrane.

In order to probe for a potential protonophoric activity of compounds **1**-**3** in live *S. aureus* cells, a pH-sensitive dye 3,3'-diethyloxacarbocyanine iodide [DiOC$_2$(3)] was first utilized. In healthy cells with polarized membranes, a significant proportion of the fluorescent green dye forms aggregates that exhibit red fluorescence and the ratio of red:green fluorescence is relatively high. When the membrane is depolarized, red fluorescence is reduced in favor of green fluorescence and the ratio of red:green fluorescence is decreased. Similar to the prototypical

10

protonophore CCCP, the addition of compounds **1-3** produced clear MIC-dependent membrane depolarization within minutes, as signified by a decrease in the red:green fluorescence ratio (Figure 4A). As often seen for ionophores, the depolarization starts at a fraction of the MIC and is already strong at the MIC, indicating that this mechanism is indeed relevant for bacterial killing.[34] Monodeoxypyoluteorin (**4**) also caused membrane depolarization in an MIC-dependent manner, but, in accordance with the higher MIC, an eightfold higher concentration than marinopyrrole (**1**) was needed to elicit the same strength of effect (Supplementary Figure S34A and Table 1). Notably, O,O'-dimethylated MarA (**8**) and N,O,O'-trimethyl MarA (**9**) produced no measurable membrane depolarization, even at high concentrations (Supplementary Figure S34A).

To further determine whether the membrane depolarization observed upon treatment of *S. aureus* cells with compounds **1-3** can be specifically attributed to protonophore activity, the ratiometric pH indicator dye 2',7'-bis-(2-carboxyethyl)-5-(and-6)-carboxyfluorescein acetoxymethyl ester (BCECF AM) was employed. Upon addition of compounds **1-3**, the intracellular pH dropped significantly in a MIC-dependent manner within minutes (Figure 4B). For MarA (**1**) at 1x MIC, the pH dropped from 7.8 to 7.5 (Δ0.3 pH units) in 10 minutes; for PBP (**2**) and PCB (**3**) at 1x MIC, the pH dropped from 7.8 to 7.6 (Δ0.2 pH units) in 10 minutes. At 4x MIC all three compounds produced an intracellular reduction in pH from 7.8 to 7.4 (Δ0.4 pH units). Remarkably, a CCCP concentration of 50 µM was required to cause a similar intracellular pH reduction as a PCP (**3**) concentration of 36 pM. Again, monodeoxypyoluteorin (**4**) exhibited MIC-dependent protonophore activity at relatively high concentrations that were consistent with its higher MIC. Very weak or no protonophore activity was observed for methylated MarA derivatives **8** and **9** (Supplementary Figure S35B).

Our last method to investigate the membrane depolarization effected by compounds **1-3** in live *B. subtilis* cells involved the cell division protein MinD, which normally localizes to the polar and septal regions of the cell. Strahl and Hamoen have shown that the loss in transmembrane potential brought about by the presence of a protonophore disrupts bacterial cellular division and,

11

more specifically, causes a dramatic delocalization of several conserved cell division proteins including MinD.[35] Therefore, we monitored the cellular localization of GFP-MinD in *B. subtilis* cells after treatment with **1**-**3** in order to confirm by an independent assay the hypothesis that these compounds are, indeed, protonophores. In untreated *B. subtilis* cells, a strong fluorescence signal from GFP-MinD can be seen in the polar region as well as the septal region (Figure 4C). After a short treatment with the natural products and the positive control CCCP, the fluorescence signal of GFP-MinD became diffuse and spotty, confirming depolarization *in vivo*. As expected, O,O',N-trimethyl MarA (**9**) did not affect the localization of GFP-MinD. Interestingly, the fluorescence of the delocalized GFP-MinD was significantly brighter in cells treated with the natural products **1**-**3** compared to cells treated with CCCP.

Finally, in order to determine whether the membrane depolarization observed upon treatment with compounds **1**–**3** involved a disruption of the integrity of cytoplasmic membrane, commonly termed "pore formation", we collected fluorescence microscope images of treated cells exposed to a mixture of two dyes, the membrane permeant green SYTO9 and the red propidium iodide, which cannot cross an intact cytoplasmic membrane. Even after exposure to MarA (**1**) and PCP (**3**) at 4x MIC, *S. aureus* cells showed only green fluorescence after SYTO9/propidium iodide staining, a result pointing toward cell membrane integrity and the absence of pores (Figure 4D). Like the protonophore CCCP, **1**-**3** markedly reduced the intensity of the green fluorescence compared to the DMSO control. By contrast, cells treated with the prototypical pore-forming antibacterial nisin and subsequently stained with SYTO9-propidium iodide showed a clear red fluorescence indicative of pore formation. Furthermore, treatment of *B. subtilis* cells with **1**-**3** did not cause the blebbing phenotype that is associated with a weakening of the peptidoglycan sacculus and tell-tale signature of vancomycin exposure (Figure 4E).
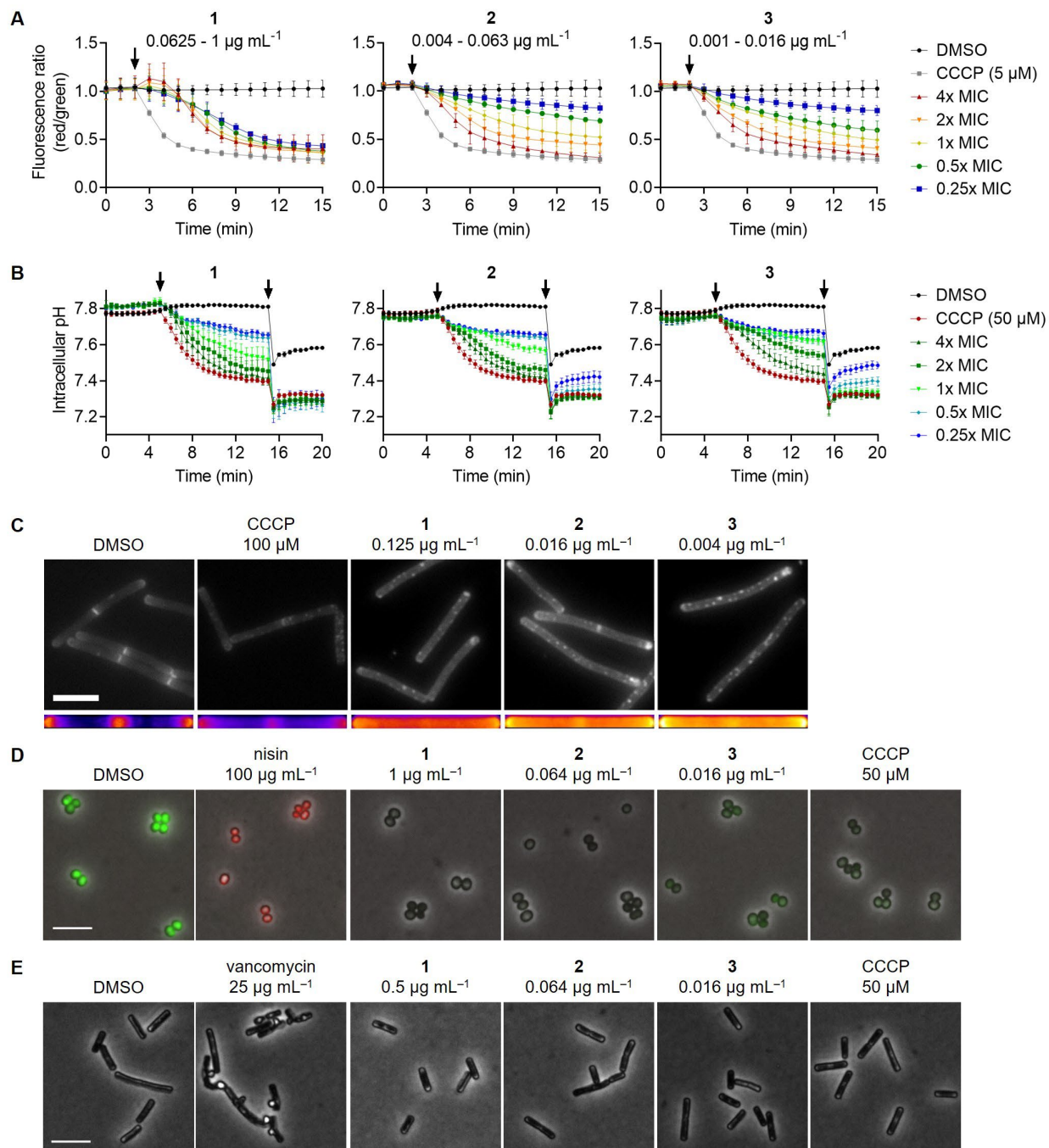
Figure 4. Compounds **1**-**3** act as protonophores. A) Time-resolved effect of **1**-**3** on the membrane potential in *S. aureus* NCTC8325 cells based on 3,3'-diethyloxacarbocyanine iodide [DiOC$_2$(3)] staining at concentrations around the respective MICs. Cells were treated with compounds **1**-**3** at 4x, 2x, 1x, 0.5x, and 0.25x MIC in the presence of DiOC$_2$(3). DMSO (1%) was used as a negative control, and CCCP (5 µM) as a positive control. Error bars indicate the standard deviation (SD) of

13

two biological replicates. The arrow shows the time point of addition of test compounds. B) Time resolved effect of **1-3** on the intracellular pH in *S. aureus* NCTC8325 cells based on 2',7'-bis-(2-carboxyethyl)-5-(and-6)-carboxyfluorescein acetoxymethyl ester (BCECF AM) staining in relation to the MICs. Cells were treated with compounds **1-3** at 4x, 2x, 1x, 0.5x, and 0.25x MIC in the presence of BCECF AM. DMSO (1%) was used as a negative control, and CCCP (50 μM) as a positive control. Error bars indicate the standard deviation (SD) of three biological replicates. The first arrow shows the time point of test compound addition; the second arrow shows the time point for adding nigericin (20 μM), a H^+/K^+ antiporter further reducing the intracellular proton concentration and equilibrating it to the external environment. C) GFP-MinD distribution in growing *B. subtilis* 168 cells after compound exposure. Cells were incubated for 10 min with compounds **1-3** at 1x MIC. DMSO (1%) was used as a negative control, and CCCP (100 μM) as a positive control. The micrographs (top row) show representative images of the fluorescence channel which were all adjusted to the same microscopy settings for direct qualitative comparison. The fluorescence heatmaps (bottom row) displays the spatial distribution of the median fluorescent GFP-MinD signal quantified from at least N ≥ 100 cells per experiment from three independent biological replicates. Warmer colors indicate stronger localization in this position. D) Effect of membrane integrity on *S. aureus* NCTC8325 after 10 min treatment with compounds **1-3** at 4x MIC visualized by SYTO9 (green) and propidium iodide (PI, red) co-staining. DMSO (1%) and CCCP (50 μM) were used as negative controls, and nisin (100 μg mL^{-1}) as a positive control. The images shown are an overlay of the brightfield, SYTO9, and PI channels. E) Brightfield visualization of the formation of cell wall blebs in *B. subtilis* 168 cells after 10 min treatment with compounds **1-3** at 4x MIC and fixation by acetic acid/methanol. DMSO (1%) was used as a negative control, and vancomycin (25 μg mL^{-1}) as a positive control. CCCP = carbonyl cyanide m-chlorophenyl hydrazone. Scale bars, 5 μm.

14

The conclusion that the antibacterial mode of action for MarA (**1**), PBP (**2**), and PCP (**3**) is tied to their protonophoric activity is supported by other evidence. First, the natural (−)-(*M*)-MarA atropisomer and the unnatural (+)-(*P*)-MarA atropisomer showed equal potency against *S. aureus*,[1] a finding that points toward a mode of action that does not involve binding to a chiral protein. Second, synthetic derivatives of **1-3** that showed enhanced antibacterial activity (low MIC) possess greater overall acidity (low pK_a) and hydrophobicity (high logD); the presence of an acidic phenol O-H or pyrrole N-H proton and a high degree of halogenation is critical for activity. For example, MarA (**1**), which showed strong protonophore activity and antibacterial activity against *S. aureus*, has a calculated pK_a = 6.9 and a calculated logD (pH 7.4) = 5.8 (PhysChem Suite, Percepta software, ACD/Labs). Dipyrrole **7**, a nonhalogenated version of MarA, is less acidic (pK_a = 7.5), less hydrophobic (logD = 3.8), and showed significantly weaker protonophore and antibacterial activity against *S. aureus* (see Figure 2). In contrast, MarA derivatives prepared by adding chlorine, fluorine, and trifluoromethyl substituents onto the marinopyrrole core structure are more acidic (pK_a = 5.7–6.9), more hydrophobic (logD = 5.5–6.3), and showed greater antibacterial activity against *S. aureus*.[23,28–30] Presumably, PBP (**2**) and PCP (**3**) are much stronger protonophores and antibacterials than MarA (**1**) because they are stronger acids, although this distinction is not borne out by calculations.

One model to explain the protonophore activity of MarA, PBP, and PCP specifies that the natural products act as proton shuttles that pick up protons at the acidic extracellular microenvironment directly outside the cell, translocate protons across the lipid bilayer, and then release protons into the neutral cytoplasm. According to the Henderson-Hasselbach equation, stronger acids would dissociate to a greater extent inside the cell and more readily dissipate the proton motive force (PMF) and decrease the membrane potential (ΔΨ), and this might explain why stronger marinopyrrole-based acids exhibit greater antibacterial activity. The hydrophobicity of this compound class ensures strong affinity for and preferential positioning in the membrane environment, and free migration seems plausible given their small size. An alternative model

15

places the hydrophobic natural products inside the membrane within a more static structure, where they associate with the hydrophobic lipid bilayer and facilitate proton translocation and PMF dissipation through an unknown mechanism.

Methods

General experimental. Compounds **1,2,4-9** were synthesized according to published procedures.[23,36,37] PCP (**3**) was synthesized using a modification of the published PBP (**2**) synthesis.[37] All other reagents and solvents were purchased commercially and were used without further purification. Compounds and reaction mixtures were analyzed on an analytical 1100 Series Agilent Technologies HPLC system coupled to UV/vis (210, 254, and 360 nm) and evaporative light-scattering detector (ELSD) using a Phenomenex Luna reversed-phase C18(2) column (100×4.6 mm, 5 μm, 100 Å) with a 10 or 20 gradient from 10–100 % CH_3CN in water containing 0.1 % formic acid and a 1.0 or 0.7 mL min^{-1} flow rate. Using the same column and a 20 min gradient from 10–100 % CH_3CN in water containing 0.1 % formic acid and a 0.7 mL min^{-1} flow rate, HPLC-ESI-QTOF-MS/MS was performed on an analytical Agilent 1260 Infinity Series LC system coupled to a 6530 Series QTOF mass spectrometer. Column chromatography was performed on a Teledyne CombiFlash Rf+ Lumen flash chromatography system. Preparative HPLC was performed using a Millipore Waters 600E solvent delivery system with a Phenomenex Luna C18(2) column (250 x 21.2 mm, 5 μm, 100 Å) and a 13 mL min^{-1} flow rate, a Phenomenex Luna C8(2) column (250 x 10 mm, 5 μm, 100 Å) and a 3 mL min^{-1} flow rate or Phenomenex Luna silica columns (250 × 21.2 mm or 250 × 10 mm, 5 μm, 100 Å) and a 13 or 3 mL min^{-1} flow rate. Compounds were detected with a single-wavelength Knauer UV detector at 254 nm or 360 nm. Infrared (IR) spectra were obtained as films on KBr discs (25 x 4 mm) using a Thermo Nicolet IR 100 FT-IR. ^{1}H and 2D NMR spectra were recorded on a Jeol 500 MHz spectrometer in CD_3OD (residual solvent referenced to 3.31 ppm). ^{13}C NMR spectra were recorded on the same instrument at 125 MHz in CD_3OD (referenced to 49.0 ppm). The following abbreviations are used

16

to indicate the multiplicity in ^{1}H NMR spectra: s = singlet, d = doublet, t = triplet, dd = doublet of doublets, td = triplet of doublets, m = multiplet, br s = broad singlet.

General procedure for 6-heptynoic acid coupling. Phenols **1-7** were dissolved in DMF (1 mL). EDC (7 eq) and DMAP (0.1 eq) were then added, followed by 6-heptynoic acid (1.2-3.0 eq) and Et$_3$N (2 eq). The reaction mixtures were stirred for 2 - 23 h at room temperature. The progress of the reactions was monitored using HPLC and TLC. The reactions were quenched by adding a saturated NH$_4$Cl solution (3 mL), and the aqueous layers were then extracted with EtOAc (3 x 3 mL). The combined EtOAc extracts were washed with brine (1 mL), dried over Na$_2$SO$_4$, filtered and concentrated to dryness. The products were purified using preparative reversed-phase HPLC.

General procedure for click reaction. Click reaction was conducted under standard conditions using alkyne (1 eq), coumarin azide (1.5 eq), CuSO$_4$ (0.1 eq), sodium ascorbate (0.2 eq) in DMF:water (1:1). The reaction mixtures were directly purified using preparative reversed-phase HPLC.

1C: C8(2) Luna, 250 x 10 mm, 65% MeCN in water (0.1% TFA), 360 nm, 3 mL min^{-1}, t$_R$ = 15 min

2C: C8(2) Luna, 250 x 10 mm, 70% MeCN in water (0.1% TFA), 360 nm, 3 mL min^{-1}, t$_R$ = 13 min

3C: C8(2) Luna, 250 x 10 mm, 65% MeCN in water (0.1% TFA), 360 nm, 3 mL min^{-1}, t$_R$ = 18 min

4C: C8(2) Luna, 250 x 10 mm, 50% MeCN in water (0.1% TFA), 360 nm, 3 mL min^{-1}, t$_R$ = 20 min

5C: C8(2) Luna, 250 x 10 mm, 45% MeCN in water (0.1% TFA), 360 nm, 3 mL min^{-1}, t$_R$ = 14 min

6C: C18(2) Luna, 250 x 10 mm, 50% MeCN in water (0.1% TFA), 360 nm, 3 mL min^{-1}, t$_R$ = 16 min

7C: C8(2) Luna, 250 x 10 mm, 55% MeCN in water (0.1% TFA), 360 nm, 3 mL min^{-1}, t$_R$ = 18 min

10: C18(2) Luna, 250 x 21.2 mm, 40% MeCN in water (0.1% TFA), 360 nm, 13 mL min^{-1}, t$_R$ = 11 min

Antimicrobial assays. Minimal inhibitory concentrations were determined by the broth microdilution method in accordance with the guidelines of the Clinical and Laboratory Standards

17

Institute (CLSI).[38] Twofold dilutions of the test compounds starting from 64 µg mL^{-1} were prepared in cation-adjusted Mueller-Hinton broth (BD Difco) in 96-well round bottom polystyrol plates (Sarstedt) with each well containing 50 µL of test compound solution at twice the final concentration. The wells were then inoculated with 50 µL of the bacterial suspension of the test strains, prepared by the direct colony suspension method, to a final inoculum of 5×10^5 colony-forming units (CFU) mL^{-1} in 100 µL final volume. The plates were incubated at 37°C for 20 h, and the minimal inhibitory concentration was determined as the lowest concentration of test compound that inhibited visible bacterial growth.

Cytotoxicity assays. Cytotoxicity evaluation was performed using a 7-hydroxy-3H-phenoxazin-3-one 10-oxide (resazurin) assay in RPMI cell culture medium (Gibco Life Technologies) supplemented with 10% heat-inactivated fetal bovine serum (Gibco Life Technologies) for the HeLa cell line and Dulbecco's Modified Eagle's Medium (DMEM) cell culture medium (Gibco Life Technologies) supplemented with 10% heat-inactivated fetal bovine serum for the A549 and MRC5 cell lines. A twofold serial dilution of the test compounds was prepared in a 96-well polystyrene microtiter plate and seeded with trypsinized HeLa, A549 or MRC5 cells to a final cell concentration of 1×10^4 cells per well. After 24 h incubation at 37°C, 5% CO_2, and 95% relative humidity, resazurin was added to a final concentration of 200 µM, and cells were again incubated overnight. Cell viability was assessed by determining the reduction of resazurin to resorufin by measuring the fluorescence in a Tecan Infinite M200 Pro reader at an excitation wavelength of 560 nm and an emission wavelength of 600 nm in relation to an untreated control.

Fluorescence microscopy. In order to monitor the localization of the coumarin derivatives, *B. subtilis* cells were grown in LB overnight at 37 °C with agitation (180 rpm), diluted 1:100 in fresh medium, and grown at 37 °C to an OD$_{600}$ of 0.3-0.4. Cells were incubated with **1C** (1 µg mL^{-1}, 1x MIC), **2C** (0.25 µg mL^{-1}, 1x MIC) or **3C** (0.25 µg mL^{-1}, 1x MIC) for 10 minutes and then washed at least four times with PBS. Coumarin **10** (8 µg mL^{-1}) was used as a negative control. All the labelling experiments were repeated three times. Subsequently, the cells were placed on

microscopy slides covered with a thin layer of agarose (1.2 % in PBS) and visualized by brightfield and fluorescence microscopy in a Zeiss Axio Observer Z1 LSM800 at λ_{ex} 353 nm / λ_{em} 465 nm. Images were acquired with an Orca Flash 4.0 V2 camera (Hamamatsu) and an α Plan-Apo 100x/1.46 Oil Ph3 objective (Zeiss). Image processing was performed in FIJI.[39]

FM 5-95 labelling after antibiotic exposure was conducted as described previously.[40] Briefly, *B. subtilis* cell were grown in LB medium at 37°C, 200 rpm to an OD_{600} of 0.3. Cells were treated with either **1** (0.125 µg mL^{-1}, 1x MIC), **2** (0.016 µg mL^{-1}, 1x MIC), **3** (0.004 µg mL^{-1}, 1x MIC), **4** (16 µg mL^{-1}, 1x MIC), **8** (32 µg mL^{-1}, 1x MIC), **9** (128 µg mL^{-1}, 30 min) or DMSO (1%) as a negative control and incubated at 37 °C for 15 min. Samples were labelled with 20 µg mL^{-1} of N-(3-trimethylammoniumpropyl)-4-(6-(4-(diethylamino)phenyl)hexatrienyl) pyridinium dibromide (FM 5-95, Molecular Probes) and visualized as described above at λ_{ex} 587 nm / λ_{em} 610 nm.

In order to visualize the cellular localization of GFP-MinD in *B. subtilis* cells, a strain harboring a GFP-*minD* construct was grown in LB overnight at 37 °C with agitation (180 rpm).[35] The culture was then diluted 1:100 in fresh medium, supplemented with 0.1% xylose (w/v) for GFP-MinD expression, and grown at 37 °C to an OD_{600} of 0.6-0.8. Cells were incubated for 10 min with compounds **1–4**, **8**, and **9** at 1x MIC. CCCP (100 µM) was used as a positive and DMSO (1%) as a negative control. Cells were visualized as described above at λ_{ex} 488 nm / λ_{em} 509 nm. To quantitatively assess the GFP-MinD localization, fluorescence heatmaps, presenting the spatial distribution of the median fluorescence the GFP-MinD signal, were created with MicrobeJ[41] from N ≥ 100 cells per experiment from three independent biological replicates.

Membrane potential assay. *S. aureus* NCTC8325 cells were grown in LB medium at 37°C with agitation (200 rpm) to an OD_{600} of 0.75. Cells were then pelleted and resuspended to an OD_{600} of 0.5 in PBS and incubated with 30 µM 3,3′-diethyloxacarbocyanine iodide (DiOC$_2$(3), Molecular Probes, Fisher Scientific) for 15 min in the dark. The loaded cells were transferred to a black 96-well flat bottom polystyrol microtiter plate (BRAND), and a baseline measurement was taken for

19

2 min at an excitation wavelength of 485 nm and two emission wavelengths, 530 nm (green) and 630 nm (red) using a microplate reader (Tecan Spark). A concentration series of the test compounds (in 1% DMSO) was added, and the measurement continued as above for 15 min. The protonophore CCCP was used as a positive control at a concentration of 5 µM, and DMSO was used as a negative control at a concentration of 1%.

Protonophore assay. *S. aureus* NCTC8325 cells were grown in LB medium at 37°C with agitation (200 rpm) to an OD_{600} of 0.8. Cells were then pelleted and resuspended in PBS and incubated with 25 µg mL^{-1} BCECF-AM dye (Molecular Probes, Fisher Scientific) for 30 min in a water bath at 30°C. Cells were washed twice with PBS buffer containing 25 mM glucose and incubated for another 5 min in a water bath at 37°C. The treated cells were transferred to a black 96-well flat bottom polystyrol microtiter plate (BRAND), and a baseline measurement was taken for 5 min at two excitation wavelengths, λ_{ex} 440 and λ_{ex} 490 nm, and one emission wavelength, λ_{em} 530 nm, using a microplate reader (Tecan Spark). A concentration series of the test compounds (in 1% DMSO) was added, and the measurement continued as above for 10 min. Then, 20 µM nigericin was added to each well, and the measurement continued for a final 5 min. The protonophore CCCP was used as a positive control at a concentration of 50 µM, and DMSO was used as a negative control at a concentration of 1%. The intracellular pH was calculated based on a calibration curve with nigericin and PBS buffer adjusted of various defined pH values.

Pore-forming assay. Pore formation was monitored using the Live/Dead BacLight bacterial viability kit (Molecular Probes). *S. aureus* NCTC8325 cells were grown in LB at 37 °C to the exponential phase. Aliquots (100 µL) of the cells were treated with **1** (1 µg mL^{-1}, 4x MIC), **2** (0.064 µg mL^{-1}, 4x MIC), **3** (0.016 µg mL^{-1}, 4x MIC), CCCP (50 µM), nisin (100 µg mL^{-1}, Sigma-Aldrich) or DMSO (1%) as a negative control. Samples were incubated for 20 min and then 0.2 µL of a 1:1 mixture of SYTO9 and propidium iodide (PI) was added per 100 µL of culture. Samples were further incubated for 15 min at room temperature in the dark before microscopic analysis.

Samples were visualized by brightfield and fluorescence microscopy at at λ_{ex} 483 nm / λ_{em} 500 nm (SYTO9) and at λ_{ex} 305 nm / λ_{em} 617 nm (PI) on microscope slides covered with a thin film of 1% agarose using a Zeiss Axio Observer Z1 automated microscope. Images were acquired with an Orca Flash 4.0 V2 camera (Hamamatsu) and an alpha Plan-Apochromat 100x/1.46 Oil Ph3 objective (Zeiss). Images were processed using the Zen software package (Zeiss).

Blebbing assay. *B.subtilis* 168 cells were grown in cation-adjusted Mueller-Hinton medium at 37 °C with agitation (200 rpm) to OD_{600} of 0.35. Aliquots (100 µL) of the cells were treated with 8x MIC of **1** (1 µg mL^{-1}, 4x MIC), **2** (0.064 µg mL^{-1}, 4x MIC), **3** (0.016 µg mL^{-1}, 4x MIC), vancomycin (2 µg mL^{-1}, 10x MIC) or DMSO (1%) as a negative control. Samples were incubated for 30 min and then 25 µL were added to a fresh tube containing 100 µL of a 1:3 (v:v) mixture of acetic acid and methanol. Samples were visualized by brightfield microscopy on microscope slides covered with a thin film of 1% agarose using a Zeiss Axio Observer Z1 automated microscope. Images were acquired with an Orca Flash 4.0 V2 camera (Hamamatsu) and an alpha Plan-Apochromat 100x/1.46 Oil Ph3 objective (Zeiss). Images were processed using the Zen software package (Zeiss).

Notes

The authors declare no conflict of interest.

Acknowledgments

References

(1)   Hughes, C. C.; Prieto-Davo, A.; Jensen, P. R.; Fenical, W. The marinopyrroles, antibiotics of an unprecedented structure class from a marine Streptomyces sp. *Org. Lett.* **2008**, *10*, 629–631. DOI:10.1021/ol702952n.

(2)   Burkholder, P. R.; Pfister, R. M.; Leitz, F. H. Production of a pyrrole antibiotic by a marine bacterium. *Appl. Microbiol.* **1966**, *14*, 649–653. DOI:10.1128/am.14.4.649-653.1966.

(3)   Lovell, F. M. The structure of a bromine-rich marine antibiotic. *J. Am. Chem. Soc.* **1966**, *88*, 4510–4511. DOI:10.1021/ja00971a040.

(4)   Cavalleri, B.; Volpe, G.; Tuan, G.; Berti, M.; Parenti, F. A chlorinated phenylpyrrole antibiotic from Actinoplanes. *Curr. Microbiol. An Int. J.* **1978**, *1*, 319–324. DOI:10.1007/BF02601691.

(5)   ApSimon, J. W.; Durham, D. G.; Rees, A. H.; Chemistry, D. Synthesis of some 2-phenylpyrrole derivatives. *J. Chem. Soc., Perkin I* **1978**, 1588–1594.

(6)   Hughes, C. C.; Yang, Y. L.; Liu, W. T.; Dorrestein, P. C.; La Clair, J. J.; Fenical, W. Marinopyrrole A target elucidation by acyl dye transfer. *J. Am. Chem. Soc.* **2009**, *131*, 12094–12096. DOI:10.1021/ja903149u.

(7)   Doi, K.; Li, R.; Sung, S. S.; Wu, H.; Liu, Y.; Manieri, W.; Krishnegowda, G.; Awwad, A.; Dewey, A.; Liu, X.; Amin, S.; Cheng, C.; Qin, Y.; Schonbrunn, E.; Daughdrill, G.; Loughran, T. P.; Sebti, S.; Wang, H. G. Discovery of marinopyrrole A (maritoclax) as a selective Mcl-1 antagonist that overcomes ABT-737 resistance by binding to and targeting Mcl-1 for proteasomal degradation. *J. Biol. Chem.* **2012**, *287*, 10224–10235. DOI:10.1074/jbc.M111.334532.

(8)   Schneider, P.; Schneider, G. De-orphaning the marine natural product (±)-marinopyrrole A by computational target prediction and biochemical validation. *Chem. Commun.* **2017**, *53*, 2272–2274. DOI:10.1039/c6cc09693j.

(9)   Fedorov, R.; Böhl, M.; Tsiavaliaris, G.; Hartmann, F. K.; Taft, M. H.; Baruch, P.; Brenner, B.; Martin, R.; Knölker, H.-J.; Gutzeit, H. O.; Manstein, D. J. The mechanism of pentabromopseudilin inhibition of myosin motor activity. *Nat. Struct. Mol. Biol.* **2009**, *16*, 80–88. DOI:10.1038/nsmb.1542.

(10)   Martin, R.; Jäger, A.; Bohl, M.; Richter, S.; Fedorov, R.; Manstein, D. J.; Gutzeit, H. O.; Knôlker, H. J. Total synthesis of pentabromo- and pentachloropseudilin, and synthetic analogues-allosteric inhibitors of myosin ATPase. *Angew. Chemie - Int. Ed.* **2009**, *48*, 8042–8046. DOI:10.1002/anie.200903743.

(11)   Chinthalapudi, K.; Taft, M. H.; Martin, R.; Heissler, S. M.; Preller, M.; Hartmann, F. K.; Brandstaetter, H.; Kendrick-Jones, J.; Tsiavaliaris, G.; Gutzeit, H. O.; Fedorov, R.; Buss, F.; Knölker, H. J.; Coluccio, L. M.; Manstein, D. J. Mechanism and specificity of pentachloropseudilin-mediated inhibition of myosin motor activity. *J. Biol. Chem.* **2011**, *286*, 29700–29708. DOI:10.1074/jbc.M111.239210.

(12)   Ohri, R. V.; Radosevich, A. T.; Hrovat, K. J.; Musich, C.; Huang, D.; Holman, T. R.; Toste, F. D. A Re(V)-catalyzed C-N bond-forming route to human lipoxygenase inhibitors. *Org. Lett.* **2005**, *7*, 2501–2504. DOI:10.1021/ol050897a.

(13)   Eichhorn, J. M.; Alford, S. E.; Hughes, C. C.; Fenical, W.; Chambers, T. C. Purported Mcl-1 inhibitor marinopyrrole A fails to show selective cytotoxicity for Mcl-1-dependent cell lines. *Cell Death Dis.* **2013**, *4*. DOI:10.1038/cddis.2013.411.

(14)   Gomez-Bougie, P.; Dousset, C.; Descamps, G.; Schnitzler, A.; Audiger, L.; Tessier, A.; Dubreuil, D.; Lebreton, J.; Pellat-Deceunynck, C.; Amiot, M. The selectivity of marinopyrrole A to induce apoptosis in MCL1high BCL2low expressing myeloma cells is related to its ability to impair protein translation. *Br. J. Haematol.* **2018**, *180*, 157–159.

DOI:10.1111/bjh.14293.

(15) Cota Teixeira, S.; Silva Lopes, D.; Santos da Silva, M.; Cordero da Luz, F. A.; Cirilo Gimenes, S. N.; Borges, B. C.; Alves da Silva, A.; Alves Martins, F.; Alves dos Santos, M.; Teixeira, T. L.; Oliveira, R. A.; de Melo Rodrigues Ávila, V.; Barbosa Silva, M. J.; Elias, M. C.; Martin, R.; Vieira da Silva, C.; Knölker, H. J. Pentachloropseudilin impairs angiogenesis by disrupting the actin cytoskeleton, integrin trafficking and the cell cycle. *ChemBioChem* **2019**, *20*, 2390–2401. DOI:10.1002/cbic.201900203.

(16) Laatsch, H.; Renneberg, B.; Hanefeld, U.; Kellner, M.; Pudleiner, H.; Hamprecht, G.; Kraemer, H.-P.; Anke, H. Structure-activity relationships of phenyl- and benzoylpyrroles. *Chem. Pharm. Bull.* **1995**, *43*, 537–546.

(17) Whalen, K. E.; Kirby, C.; Nicholson, R. M.; O'Reilly, M.; Moore, B. S.; Harvey, E. L. The chemical cue tetrabromopyrrole induces rapid cellular stress and mortality in phytoplankton. *Sci. Rep.* **2018**, *8*, 1–11. DOI:10.1038/s41598-018-33945-3.

(18) Xiao, Y.; Yang, J.; Zou, L.; Wu, P.; Li, W.; Yan, Y.; Li, Y.; Li, S.; Song, H.; Zhong, W.; Qin, Y. Synthesis of 10,10′-bis(trifluoromethyl) marinopyrrole A derivatives and evaluation of their antiviral activities in vitro. *Eur. J. Med. Chem.* **2022**, *238*. DOI:10.1016/j.ejmech.2022.114436.

(19) Kunfermann, A.; Witschel, M.; Illarionov, B.; Martin, R.; Rottmann, M.; Höffken, H. W.; Seet, M.; Eisenreich, W.; Knölker, H. J.; Fischer, M.; Bacher, A.; Groll, M.; Diederich, F. Pseudilins: Halogenated, allosteric inhibitors of the non-mevalonate pathway enzyme IspD. *Angew. Chemie - Int. Ed.* **2014**, *53*, 2235–2239. DOI:10.1002/anie.201309557.

(20) Martens, M. C.; Liu, Y.; Sanford, A. G.; Wallick, A. I.; Warner, R. C.; Li, R.; Davis, P. H. Analogs of marinopyrrole A show enhancement to observed in vitro potency against acute Toxoplasma gondii infection. *Antimicrob. Agents Chemother.* **2022**, *66*. DOI:10.1128/AAC.00794-21.

(21) Spirandelli da Costa, M.; Borges, B. C.; Marques, I. T.; de Oliveira, R. C.; Teixeira, T. L.;

de Gouveia Santos, J.; da Silva, C. V. Pentachloropseudilin treatment impairs host cell invasion by Trypanosoma cruzi. *ChemBioChem* **2022**, *23*, 2–5. DOI:10.1002/cbic.202200349.

(22)   Haste, N. M.; Hughes, C. C.; Tran, D. N.; Fenical, W.; Jensen, P. R.; Nizet, V.; Hensler, M. E. Pharmacological properties of the marine natural product marinopyrrole A against methicillin-resistant Staphylococcus aureus. *Antimicrob. Agents Chemother.* **2011**, *55,* 3305–3312. DOI:10.1128/AAC.01211-10.

(23)   Hughes, C. C.; Kauffman, C. A.; Jensen, P. R.; Fenical, W. Structures, reactivities, and antibiotic properties of the marinopyrroles A−F. *J. Org. Chem.* **2010**, *75*, 3240–3250. DOI:10.1021/jo1002054.

(24)   Peach, K. C.; Bray, W. M.; Winslow, D.; Linington, P. F.; Linington, R. G. Mechanism of action-based classification of antibiotics using high-content bacterial image analysis. *Mol. Biosyst.* **2013**, *9*, 1837–1848. DOI:10.1039/c3mb70027e.

(25)   Valderrama, K.; Pradel, E.; Firsov, A. M.; Drobecq, H.; Roy, H. B.; Baptiste, V.; Antonenko, Y. N.; Hartkoorn, R. C. Pyrrolomycins are potent natural protonophores. *Antimicrob. Agents Chemother.* **2019**, *63*, 1–15.

(26)   Lacerna, N. M.; Miller, B. W.; Lim, A. L.; Tun, J. O.; Robes, J. M. D.; Cleofas, M. J. B.; Lin, Z.; Salvador-Reyes, L. A.; Haygood, M. G.; Schmidt, E. W.; Concepcion, G. P. Mindapyrroles A-C, pyoluteorin analogues from a shipworm-associated bacterium. *J. Nat. Prod.* **2019**, *82*, 1024–1028. DOI:10.1021/acs.jnatprod.8b00979.

(27)   Arisetti, N.; Fuchs, H. L. S.; Coetzee, J.; Orozco, M.; Ruppelt, D.; Bauer, A.; Heimann, D.; Kuhnert, E.; Bhamidimarri, S. P.; Bafna, J. A.; Hinkelmann, B.; Eckel, K.; Sieber, S. A.; Müller, P. P.; Herrmann, J.; Müller, R.; Winterhalter, M.; Steinem, C.; Brönstrup, M. Total synthesis and mechanism of action of the antibiotic armeniaspirol A. *Chem. Sci.* **2021**, *12*, 16023–16034. DOI:10.1039/d1sc04290d.

(28)   Liu, Y.; Haste, N. M.; Thienphrapa, W.; Nizet, V.; Hensler, M.; Li, R. Marinopyrrole

derivatives as potential antibiotic agents against methicillin-resistant Staphylococcus aureus (I). *Mar. Drugs* **2012**, *10*, 953–962. DOI:10.3390/md10040953.

(29) Cheng, C.; Liu, Y.; Song, H.; Pan, L.; Li, J.; Qin, Y.; Li, R. Marinopyrrole derivatives as potential antibiotic agents against methicillin-resistant staphylococcus aureus (II). *Mar. Drugs* **2013**, *11*, 2927–2948. DOI:10.3390/md11082927.

(30) Liu, Y.; Haste, N. M.; Thienphrapa, W.; Li, J.; Nizet, V.; Hensler, M.; Li, R. Marinopyrrole derivatives as potential antibiotic agents against methicillin-resistant Staphylococcus aureus (III). *Mar. Drugs* **2014**, *12*, 2458–2470. DOI:10.3390/md12052458.

(31) Zhang, L.; Esquembre, L. A.; Xia, S.-N.; Oesterhelt, F.; Hughes, C. C.; Brötz-Oesterhelt, H.; Teufel, R. Antibacterial synnepyrroles from human-associated Nocardiopsis sp. show protonophore activity and disrupt the bacterial cytoplasmic membrane. *ACS Chem. Biol.* **2022**, *17*, 2836–2848. DOI:10.1021/acschembio.2c00460.

(32) Mendes, S. S.; Marques, J.; Mesterházy, E.; Straetener, J.; Arts, M.; Pissarro, T.; Reginold, J.; Berscheid, A.; Bornikoel, J.; Kluj, R. M.; Mayer, C.; Oesterhelt, F.; Friães, S.; Royo, B.; Schneider, T.; Brötz-Oesterhelt, H.; Romão, C. C.; Saraiva, L. M. Synergetic Antimicrobial Activity and Mechanism of Clotrimazole-Linked CO-Releasing Molecules. *ACS Bio Med Chem Au* **2022**, *2*, 419–436. DOI:10.1021/acsbiomedchemau.2c00007.

(33) Gänzle, M.; Vogel, R. Studies on the mode of action of reutericyclin. *Appl. Environ. Microbiol.* **2003**, *69*, 1305–1307. DOI:10.1016/0926-6550(62)90075-0.

(34) Zipperer, A.; Konnerth, M. C.; Laux, C.; Berscheid, A.; Janek, D.; Weidenmaier, C.; Burian, M.; Schilling, N. A.; Slavetinsky, C.; Marschal, M.; Willmann, M.; Kalbacher, H.; Schittek, B.; Brötz-Oesterhelt, H.; Grond, S.; Peschel, A.; Krismer, B. Human commensals producing a novel antibiotic impair pathogen colonization. *Nature* **2016**, *535*, 511–516. DOI:10.1038/nature18634.

(35) Strahl, H.; Hamoen, L. W. Membrane potential is important for bacterial cell division. *Proc. Natl. Acad. Sci. U. S. A.* **2010**, *107*, 12281–12286. DOI:10.1073/pnas.1005485107.

(36) Nicolaou, K. C.; Simmons, N. L.; Chen, J. S.; Haste, N. M.; Nizet, V. Total synthesis and biological evaluation of marinopyrrole A and analogs. *Tetrahedron Lett.* **2011**, *52*, 2041–2043. DOI:10.1016/j.tetlet.2010.09.059.

(37) Kum, D. Y.; Nazari, M.; McPhail, K. L.; Cooper, C. S.; Suyama, T. L. Two-step total synthesis of an anti-MRSA and myosin-inhibiting marine natural product pentabromopseudilin via Suzuki-Miyaura coupling of a MIDA boronate ester. *Tetrahedron Lett.* **2017**, *58*, 3374–3376. DOI:10.1016/j.tetlet.2017.07.057.

(38) Methods for dilution antimicrobial susceptibility tests for bacteria that grow aerobically: M07-A10; approved standard. (Committee for Clinical Laboratory Standards, 2015).

(39) Schindelin, J.; Arganda-Carreras, I.; Frise, E.; Kaynig, V.; Longair, M.; Pietzsch, T.; Preibisch, S.; Rueden, C.; Saalfeld, S.; Schmid, B.; Tinevez, J. Y.; White, D. J.; Hartenstein, V.; Eliceiri, K.; Tomancak, P.; Cardona, A. Fiji: An open-source platform for biological-image analysis. *Nat. Methods* **2012**, *9*, 676–682. DOI:10.1038/nmeth.2019.

(40) Mayer, C.; Sass, P.; Brötz-Oesterhelt, H. Consequences of dosing and timing on the antibacterial effects of ADEP antibiotics. *Int. J. Med. Microbiol.* **2019**, *309*. DOI:10.1016/j.ijmm.2019.151329.

(41) Ducret, A.; Quardokus, E. M.; Brun, Y. V. MicrobeJ, a tool for high throughput bacterial cell detection and quantitative analysis. *Nat. Microbiol.* **2016**, *1*, 1–7. DOI:10.1038/nmicrobiol.2016.77.